



1 **The impact of aerosols on photolysis frequencies and ozone**
2 **production in urban Beijing during the four-year period**
3 **2012–2015**

4 Wenjie Wang¹, Min Shao^{1,2*}, Min Hu¹, Limin Zeng¹, Yusheng Wu¹

5

6 1 State Joint Key Laboratory of Environmental Simulation and Pollution Control,
7 College of Environmental Sciences and Engineering, Peking University, Beijing
8 100871, China

9 2 Institute for Environmental and Climate Research, Jinan University, Guangzhou
10 511443, China

11

12

13

14

15

16

17 *** Correspondence to:**

18 Prof. Min SHAO

19 College of Environmental Sciences and Engineering, Peking University, Beijing
20 100871, China

21 Tel: +86-10-62757973; Fax: +86-10-62757973

22 Email: mshao@pku.edu.cn



23 **Abstract**

24 During the period 2012-2015, the photolysis frequencies were measured at the
25 Peking University site (PKUERS), a representative site of urban Beijing. We present a
26 study of the effects of aerosols on two key photolysis frequencies, $j(\text{O}^1\text{D})$ and $j(\text{NO}_2)$.
27 Both $j(\text{O}^1\text{D})$ and $j(\text{NO}_2)$ display significant dependence on AOD with a nonlinear
28 negative correlation. With the increase in AOD, the slopes of photolysis frequencies
29 vs AOD decrease, which indicates that the capacity of aerosols to reduce the actinic
30 flux decreases with AOD. In addition, the slopes are equal to $4.21\text{-}6.93\cdot 10^{-6} \text{ s}^{-1}$ and
31 $3.20\cdot 10^{-3} \text{ s}^{-1}$ per AOD unit for $j(\text{O}^1\text{D})$ and $j(\text{NO}_2)$ respectively at SZA of 60° , both of
32 which are larger than those observed in the Mediterranean. This indicates that the
33 aerosols in urban Beijing have a stronger extinction on actinic flux than absorptive
34 dust aerosols in the Mediterranean. Since the photolysis frequencies strongly
35 depended on the AOD and the solar zenith angle (SZA), we established a parametric
36 equation to quantitatively evaluate the effect of aerosols on photolysis frequencies in
37 Beijing. According to the parametric equation, aerosols lead to a decrease in $j(\text{NO}_2)$
38 by 24.2% and 30.4% for summer and winter, respectively, and the corresponding
39 decrease in $j(\text{O}^1\text{D})$ by 27.3% and 32.6% respectively, compared to an aerosol-free
40 atmosphere. Based on an observation campaign in August 2012, we used the
41 photochemical box model to simulate the ozone production rate ($P(\text{O}_3)$). The
42 simulation results shows that the monthly average net ozone production rate is
43 reduced by up to 25% due to the light extinction of aerosols. Through further in-depth
44 analysis, it was found that particulate matter concentrations maintain high level under



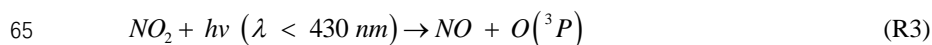
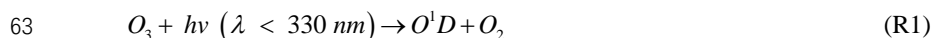
45 the condition of high concentrations of ozone precursors (VOCs and NO_x), which
46 inhibits the production of ozone to a large extent. This phenomenon implies a
47 negative feedback mechanism in the atmospheric environment of urban Beijing.

48

49

50 **1. Introduction**

51 Solar radiation plays an important role in atmospheric photochemistry, driving
52 the photolysis of many key species. The photolysis of ozone (O₃), gaseous nitrous
53 acid (HONO), and carbonyl species, which contributes to the primary production of
54 HO_x (Volkamer et al., 2010). The photolysis of ozone produces O¹D, which then
55 reacts with H₂O to form OH radicals; these radicals are the main source of OH
56 radicals in the troposphere, as shown by reactions R1 and R2. The strong dependence
57 of OH concentration on j(O¹D) was found in a number of field measurements (Ehhalt
58 et al., 2000; Rohrer et al., 2014; Stone et al., 2012). In addition, the photolysis of NO₂
59 produces O³P, and then O³P reacts with O₂ to produce O₃, as shown by reactions R3
60 and R4, which is the only significant source of ozone in the troposphere
61 (Finlayson-Pitts et al., 2000). The photolysis frequencies of R1 and R3 are j(O¹D) and
62 j(NO₂), respectively.





67 The photolysis frequencies are calculated by the following formula:

68
$$j = \int_{\lambda_1}^{\lambda_2} F(\lambda) \sigma(\lambda, S, T) \phi(\lambda, S, T) d\lambda$$
 (E1)

69 $F(\lambda)$ is the actinic flux dependent on wavelength. $\sigma(\lambda, S, T)$ is the absorption
70 cross section of the species that absorbs in the wavelength range λ_1 - λ_2 . $\phi(\lambda, S, T)$ is
71 the quantum yield of the photodissociation reaction product. λ , S and T represent
72 wavelength, species and temperature, respectively.

73 The effect of aerosols on photolysis frequencies depends on the aerosol optical
74 properties, SZA and altitude (Liao et al., 1999). The aerosol optical depth (AOD)
75 characterizes the integral of the extinction coefficient of aerosols in the vertical
76 direction. The light extinction of aerosols includes scattering and absorption, which
77 have different effects on the actinic flux. Scattering aerosols can enhance the actinic
78 flux throughout the troposphere, while absorptive aerosols reduce the actinic flux
79 throughout the boundary layer (Jacobson, 1998; Dickerson et al., 1997; Castro et al.,
80 2001). To distinguish between these two components, single scattering albedo (SSA)
81 is defined as the ratio of the scattering coefficient to the total extinction coefficient. In
82 areas with severe aerosol pollution, aerosols can significantly affect photolysis
83 frequencies and ozone production. Studies in Los Angeles (Jacobson, 1998), Mexico
84 City (Castro et al., 2001; Raga et al., 2001; Li et al., 2011), São Paulo (de Miranda et
85 al., 2005), Huston (Flynn et al., 2010), Europe (Real et al., 2011) and Russia (Pere et
86 al., 2015) have found that aerosols reduce ozone concentration by 5-30% by
87 attenuating photolysis frequencies. Studies in the eastern United States have shown



88 that scattering aerosols increase ozone concentration by 5-60% by increasing the
89 photolysis frequencies (Dickerson et al., 1997; He and Carmichael, 1999). Therefore,
90 it is necessary to quantitatively evaluate the effect of aerosols on photolysis
91 frequencies for the purpose of effective ozone prevention.

92 Currently, the methods for quantitatively evaluating the influence of aerosols on
93 photolysis frequencies mainly include radiative transfer model and parameterization
94 method (Madronich et al., 1993). Radiative transfer model is based on an algorithm
95 for calculating solar radiation and photolysis frequencies (Madronich et al., 1999).
96 The observed data of related influential factors of the photolysis frequencies are taken
97 as the model's input and the photolysis frequencies simulated are compared with the
98 observed value to test the simulation effect. The method comprehensively considers
99 the influence of aerosol optical properties on the photolysis frequencies, but it does
100 not necessarily reflect the true quantitative relationship in the atmosphere due to
101 complicated environmental conditions and thus the simulated results don't necessarily
102 reproduce observed values well (Lefer et al., 2003; Shetter et al., 2003; Hofzumahaus
103 et al., 2004). For example, the simulated slope of $j(\text{O}^1\text{D})$ vs AOD by Fast-JX
104 algorithm within the CHIMERE model was significantly smaller than the observed
105 slope, particularly for the high SZA values (Mailler et al., 2016). The parameterization
106 method is based on the observation data taken from a certain region and is used to
107 establish the parameterized relationship between the photolysis frequencies and
108 optical properties of aerosols (such as AOD). The method can reflect the actual
109 atmospheric environment conditions; it also considers less influential factors and thus



110 is easy to apply (Casasanta et al., 2011; Gerasopoulos et al., 2012). The disadvantage
111 of this method is that the established parametric equations apply only to a specific
112 region and cannot be extended to other regions.

113 With rapid economic development and urbanization in past decades, China's
114 atmospheric pollution has become more and more severe, characterized by high
115 concentrations of particulate matter and ozone. Satellite observations indicates that
116 both the particulate matter and the ozone of eastern China are at higher levels
117 compared with other locations in the globe (Verstraeten et al., 2015; Ma et al., 2014).
118 Levels of pollution in the Beijing–Tianjin–Hebei are even more severe (Chang et al.,
119 2009; Che et al., 2008; Zhang et al., 2014, Zhang et al., 2016). Therefore, it is
120 necessary to study the effects of aerosols on photolysis frequencies and ozone
121 production in the urban areas of China.

122 Previous model studies have shown that aerosols in China can affect ozone
123 production by changing the photolysis rate. Tang et al. (2004) used a sulfur
124 transmission–emission model (STEM) to discover that ozone concentration in
125 northeastern China was reduced by 0.1–0.8% in the sandstorm due to the change in
126 photolysis rate. Tie et al. (2005) used a global aerosol–chemical model to show that
127 aerosols caused $j(\text{O}^1\text{D})$ and $j(\text{NO}_2)$ to decrease in winter by 20%-30% and 10%-30%,
128 respectively, and in summer by 5%-20% and 1%-10%, respectively, resulting in 2%-5%
129 and 2% reductions in ozone concentration in winter and summer, respectively. Li et al.
130 (2011) used an air quality model to estimate the changes in the photolysis rate caused
131 by sulfate, nitrate, ammonium, and mineral dust aerosols in the central and eastern



132 regions of China from June 1 to June 12, 2006. This study showed that the daily
133 average $j(\text{O}^1\text{D})$ in the troposphere at the altitude of 1 km, 3 km, and 10 km from the
134 ground was reduced by 53.3%, 37.2%, and 20.9%, respectively, resulting in a
135 decrease in the ozone concentration by 5.4%, 3.8%, and 0.1% in the three layers. Lou
136 et al (2014) found that with aerosols, annual mean photolysis rates, $j(\text{O}^1\text{D})$ and
137 $j(\text{NO}_2)$, were simulated to be reduced by 6-18% in polluted eastern China, leading to
138 reductions in O_3 of up to 0.5 ppbv in those regions in spring and summer by using the
139 global chemical transport model (GEOS-Chem). However, all of these studies base
140 their results on model simulations. Research using long-term observational data to
141 evaluate the effects of aerosols on photolysis frequencies and ozone production in
142 China has not yet been published.

143 Our overall goal is to quantitatively evaluate the effect of aerosols in urban
144 Beijing on photolysis frequencies and thus on ozone production. First, the relationship
145 between $\text{PM}_{2.5}$ and AOD was investigated. Second, based on long-term observations
146 (2012-2015) of photolysis frequencies, we discussed the impact of AOD on photolysis
147 frequencies ($j(\text{O}^1\text{D})$ and $j(\text{NO}_2)$) in urban Beijing in detail. Then, the quantitative
148 relationship between photolysis frequencies, AOD, and SZA was acquired by the
149 parameterization method, which could be used to quantitatively evaluate the effect of
150 AOD on photolysis frequencies in Beijing. Finally, a photochemistry box model was
151 used to evaluate the effect of aerosols on ozone production.



152 **2. Methodology**

153 **2.1. Measurement**

154

155 From 2012 to 2015, $j(\text{O}^1\text{D})$ and $j(\text{NO}_2)$ were measured continuously at PKUERS
156 site. The site (39.99°N, 116.31°E) is located on the sixth floor of a campus building at
157 the Peking University, 20 km northwest of Tiananmen Square. The height from the
158 ground is about 30 m. The sampling point is surrounded by classroom buildings.
159 Concentration level and composition of air pollutants were thought to be similar to the
160 downtown so as to be representative for the whole of Beijing (Wang et al., 2010; Xu
161 et al., 2011; Zhang et al., 2012; Zhang et al., 2014).

162 The actinic flux was measured using a spectroradiometer and the photolysis
163 frequencies were calculated from the absorption cross section and quantum yield of
164 each species (Shetter and Muler, 1999). The spectroradiometer consisted of a single
165 monochromator with a fixed grating (CARL ZEISS), an entrance optic with a 2π
166 steradian (sr) solid angle quartz diffusor and a flexible optical quartz fiber bundle
167 connecting both components. The spectral measurements were performed with a
168 wavelength resolution of 2 nm, covering a wavelength range of 290-650 nm
169 (Hofzumahaus et al., 1999). The measured spectra were corrected for dark signal and
170 stray light. Descriptions of the calibration procedure and calculation of photolysis
171 frequencies are given in Bohn et al.(2008). The calculated photolysis frequencies had
172 a time resolution of 10 s and an uncertainty of $\pm 10\%$.



173 The optical properties of aerosols were measured by a CIMEL solar photometer
174 (AERONET level 2 data collection, <http://aeronet.gsfc.nasa.gov/>) and the site selected
175 was the Beijing-CAMS site (39.933°N, 116.317°E), which is close to the PKUERS
176 site. The CIMEL solar photometer is an automatic solar-sky scanning radiometer that
177 uses selected spectral channels. The instrumentation, data acquisition, retrieval
178 algorithms, and calibration procedure conform to the standards of the AERONET
179 global network and have been described in detail by Fotiadi et al. (2006). The solar
180 extinction measurement was performed every 3 minutes in the spectral range 340–
181 1020 nm for the calculation of AOD at wavelengths 340, 380, 440, 500, 675, 870, 970,
182 and 1020 nm. Under cloudless conditions, the overall uncertainty of AOD data is $\pm 1\%$
183 at $\lambda > 440$ nm and ± 0.02 at shorter wavelengths. In this study, AOD at the wavelength
184 of 380 nm was chosen for analysis. This wavelength was selected as it is more
185 representative of $j(\text{NO}_2)$. The SSA data were derived from a field campaign
186 undertaken in August 2012. The absorption and scattering coefficients were measured
187 with an Aethalometer (AE-31, Magee) and a Single Wavelength Integrating
188 Nephelometer (Aurora-1000), respectively, with a time resolution of 1 minute.
189 Five-minute averages of ozone column concentration, SSA, and photolysis
190 frequencies were analyzed in this study. The total ozone column was obtained by OMI
191 (Ozone Monitoring Instrument) for the year 2012-2015, using overpass data.

192 The analysis of the effects of aerosols on ozone production (Section 3.4) was
193 based on the field campaign undertaken in August 2012. The relevant contents and
194 methods of observation are shown in Table 1. In addition, meteorological parameters



195 such as temperature, humidity, and pressure were simultaneously observed at the site.
196 Since the time resolution of VOCs is 1 hour, all data analyzed in Section 3.4 was
197 processed as 1-hour average values. In this study, we focused on the effects of
198 aerosols on photolysis frequencies and ozone production under cloudless conditions.

199 **2.2 Radiative Transfer Model Description**

200 We use the Tropospheric Ultraviolet and Visible (TUV) radiation model provided
201 by Sasha Madronich (Madronich, 1993). In order to solve the radiative transfer
202 equation, TUV uses the discrete-ordinates algorithm (DISORT) with 16 streams and
203 calculate the global irradiance spectra in 0.15 nm steps and resolution. The key
204 aerosol optical properties including AOD, SSA and AE are input into the model to test
205 the effect of aerosols on photolysis frequencies.

206 **2.3 Photochemical box model**

207 The photochemical box model used in this study is based on a regional
208 atmospheric chemical mechanism (RACM2) described by Goliff et al. (2013). The
209 mechanism includes 17 stable inorganic compounds, 4 intermediate inorganic
210 compounds, 55 stable organic compounds, and 43 intermediate organic compounds.
211 Compounds not specifically treated in RACM are incorporated into species with
212 similar functional groups. The isoprene-related mechanism used in this model is LIM
213 mechanism proposed by Peeters et al. (2009). In this study, the observed NO₂, CO,
214 SO₂, C₂–C₁₂ NMHCs, HCHO, photolysis frequencies, temperature, pressure, and
215 relative humidity were used as constraints to simulate the concentrations of reactive



216 radicals (RO_2 , HO_2 , and OH), intermediate species, and associated reaction rate
 217 constants. HONO wasn't measured during the period and was calculated according to
 218 the concentration of NO_2 and the observed ratio of HONO to NO_2 at an urban site in
 219 Beijing, which had a marked diurnal cycle, a maximum in the early morning (ratio
 220 values up to ~ 0.05 – 0.08 in summer) and a decrease during daytime to values around
 221 0.01 – 0.02 (Hendrick et al., 2014). The model was spun up for two days once it started
 222 running in order to ensure that the simulation was stable. It was assumed that the
 223 lifetime of simulated species removed by dry deposit was 24 hours. The lifetime
 224 corresponds to the assumed deposit rate of 1.2 cm s^{-1} and a well-mixed boundary
 225 layer height of about 1 km (Lu et al., 2012). Net ozone production is equal to the
 226 reaction rate between peroxy radicals (RO_2 and HO_2) and NO minus the loss rate of
 227 NO_2 and O_3 as shown in E2, E3, and E4. The ozone production rate ($P(\text{O}_3)$), the ozone
 228 loss rate ($D(\text{O}_3)$), and the net $P(\text{O}_3)$ were calculated from the simulation results.

229

$$230 \quad P(\text{O}_3) = k_{\text{HO}_2+\text{NO}} [\text{HO}_2][\text{NO}] + \sum (k_{\text{RO}_2+\text{NO}}^i [\text{RO}_2^i][\text{NO}]) \quad (\text{E2})$$

231

$$232 \quad D(\text{O}_3) = (\theta j(O^1D) + k_{\text{OH}+\text{O}_3} [\text{OH}] + k_{\text{HO}_2+\text{O}_3} [\text{HO}_2] + \sum (k_{\text{alkene}+\text{O}_3}^j [\text{alkene}^j])) [\text{O}_3] + k_{\text{OH}+\text{NO}_2} [\text{OH}][\text{NO}_2] \quad (\text{E3})$$

233

$$234 \quad \text{net } P(\text{O}_3) = P(\text{O}_3) - D(\text{O}_3) \quad (\text{E4})$$

235



236 **3. Results and discussion**

237

238 **3.1 The correlation between PM_{2.5} and AOD**

239 In order to evaluate the extinction capacity of near-surface PM_{2.5}, we
240 investigated the relationship between PM_{2.5} and AOD (at 380nm). The factors that
241 affect this relationship include aerosol type, aerosol size distribution, aerosol
242 distribution in the vertical direction, relative humidity (RH) and planetary boundary
243 layer height (PBLH) (van Donkelaar et al., 2010). Figure 1 shows the correlation
244 between AOD and PM_{2.5} in four different seasons. The determination coefficient (r^2)
245 is 0.53, 0.58, 0.62 and 0.59 for spring (March, April and May), summer (June, July
246 and August), autumn (September, October and November) and winter (December,
247 January and February), respectively. Meanwhile, the correlation exhibits significant
248 seasonal differences, having relatively smaller slope (23.56) in summer and relatively
249 larger slope (73.76) in winter (Table 2). This implies that the aerosols in summer have
250 stronger extinction capacity in summer than in winter. One reason for the seasonal
251 differences is the variation in RH among different seasons. There is higher RH in
252 summer (57.2% on average) than in winter (30.4% on average), leading to stronger
253 hygroscopic growth of aerosol particles, and thus resulting in higher scattering ability
254 of aerosol particles. According to another study in urban Beijing, the higher the RH,
255 the smaller the slope, and the higher the PBLH, the smaller the slope. In addition, the
256 slope was smaller for scattering-dominant aerosols than for absorbing-dominant



257 aerosols, and smaller for coarse mode aerosols than for fine mode aerosols (Zheng, C.
258 W et al., 2017). The slopes of the correlation between AOD (at 550nm) and PM_{2.5} in
259 this study in summer and winter are equal to 42.2 μg m⁻³ and 119.2 μg m⁻³, respectively,
260 close to that from Ma et al. (2016) (54.9 μg m⁻³ and 110.5 μg m⁻³) and Xin et al. (2016)
261 (55.2 μg m⁻³ and 93.4 μg m⁻³), but smaller significantly than that from Zheng et al.
262 (2017) (65~74 μg m⁻³ and 143~158 μg m⁻³). The differences mainly depend on the
263 aerosol composition and size distribution at different observational sites in Beijing.
264 Compared with other cities in North China (Tianjin, Shijiazhuang and Baoding) (Ma
265 et al., 2016), the slope in Beijing for winter is significantly higher, indicating that the
266 extinction capacity of aerosols in Beijing is weaker in winter.

267

268

269 **3.2 Seasonal and diurnal variability of AOD and photolysis frequencies**

270 The diurnal cycles of AOD is shown in Figure 2. AOD displays obvious diurnal
271 variation, with relatively high level at noon and low level at dawn and evening. The
272 diurnal variation of PM_{2.5} is opposite to AOD. The opposite diurnal variation of AOD
273 and PM_{2.5} is mainly due to higher development of planetary boundary layer at noon,
274 resulting in more complete mixture of particulate matter in the vertical direction. In
275 addition, AOD has obvious seasonal differences, with the highest AOD in summer
276 and the lowest AOD in winter. Conversely, PM_{2.5} in winter (66.9 μg m⁻³) is
277 significantly higher than in summer (45.5 μg m⁻³). In spite of lower PM_{2.5} in summer,
278 AOD in summer is higher due to stronger extinction capacity of PM_{2.5} as discussed in



279 3.1. Figure 3 shows the diurnal variation of the photolysis frequencies under cloudless
280 conditions for each season. $j(\text{O}^1\text{D})$ and $j(\text{NO}_2)$ are both highest in summer, followed
281 by spring and autumn, and lowest in winter. This seasonal difference is mainly
282 determined by the difference in SZA for the four seasons.

283 The observed photolysis frequencies at this site are lower than that observed in
284 the eastern Mediterranean (Crete, Greece, $35^\circ 20' \text{N}, 25^\circ 40' \text{E}$) (Gerasopoulos et al.,
285 2012) by $7.8 \times 10^{-6} \text{ s}^{-1}$ and $4.9 \times 10^{-6} \text{ s}^{-1}$ for $j(\text{O}^1\text{D})$, and $1.9 \times 10^{-3} \text{ s}^{-1}$ and $3.3 \times 10^{-3} \text{ s}^{-1}$ for
286 $j(\text{NO}_2)$, in summer and winter respectively. The corresponding lower photolysis
287 frequencies of Beijing than the eastern Mediterranean due to SZA difference is $1.7 \times$
288 10^{-6} s^{-1} and $3.0 \times 10^{-6} \text{ s}^{-1}$ for $j(\text{O}^1\text{D})$, and $8.0 \times 10^{-5} \text{ s}^{-1}$ and $6.6 \times 10^{-4} \text{ s}^{-1}$ for $j(\text{NO}_2)$
289 according to TUV model, which are significantly lower than observed decreased
290 magnitudes. Taking into account the similar levels of ozone column concentration in
291 the two sites, the large gap of photolysis frequencies in the two sites is mainly
292 attributed to the higher AOD in Beijing (0.76 ± 0.75) than in the eastern Mediterranean
293 (0.27 ± 0.13).

294 It can be seen from Figure 3 that the difference between winter and summer for
295 $j(\text{O}^1\text{D})$ is significantly larger than that for $j(\text{NO}_2)$, where the summer midday averages
296 of $j(\text{O}^1\text{D})$ and $j(\text{NO}_2)$ are 5 times and 2 times those of winter, respectively. There are
297 two reasons for this phenomenon. One, compared with $j(\text{NO}_2)$, $j(\text{O}^1\text{D})$ is more
298 sensitive to the change in SZA and the same change in SZA results in a larger change
299 in $j(\text{O}^1\text{D})$ than $j(\text{NO}_2)$. Two, the main influential factors of $j(\text{NO}_2)$ under cloudless
300 conditions are SZA and AOD, and the influence of ozone column concentration and



301 temperature on $j(\text{NO}_2)$ is negligible. However, $j(\text{O}^1\text{D})$ is affected significantly by the
302 ozone column concentration and temperature, in addition to SZA and AOD. The
303 higher ozone column concentration and lower temperature in winter than in summer
304 lead to the difference in $j(\text{O}^1\text{D})$ further increasing.

305

306

307 **3.3 The correlation between photolysis frequencies and AOD**

308 **3.3.1 The correlation between $j(\text{O}^1\text{D})$ and AOD**

309 In order to rule out the effect of SZA on photolysis frequencies, we chose SZA
310 equal to 30° and 60° ($\pm 1^\circ$) for analysis. Figure 4 presents the dependence of $j(\text{O}^1\text{D})$
311 on AOD at different levels of ozone column concentration at SZA of 30° and 60° (\pm
312 1°). The ozone column concentration has a classification width of 30 DU. $j(\text{O}^1\text{D})$
313 exhibits a clear dependence on AOD, with a nonlinear negative correlation. As AOD
314 increased, the slope of $j(\text{O}^1\text{D})$ -AOD gradually decreases, indicating that the ability of
315 aerosols to reduce $j(\text{O}^1\text{D})$ gradually decreases with AOD. This result differs from that
316 found in Mediterranean, where $j(\text{O}^1\text{D})$ was linearly negatively correlated with AOD
317 (Casasanta et al., 2011; Gerasopoulos., 2012). A larger variation range of AOD in
318 Beijing (0-3) compared with Mediterranean (0-0.6) is one reason for the difference.

319 For further analysis, the observed relation between $j(\text{O}^1\text{D})$ and AOD was
320 compared with TUV-simulated results. Panels a and b of Figure 5 present the
321 comparison between observed and TUV-simulated $j(\text{O}^1\text{D})$ against AOD at a SZA of



322 30° and 60° respectively and ozone column concentration of 330-360 DU. At low
323 AOD level (< 0.8), the observed slope of $j(\text{O}^1\text{D})$ vs AOD is significantly larger than
324 the simulated slope at SSA of 0.95, and slightly larger than the simulated slope at SSA
325 of 0.85. With AOD increasing, the observed slope decreases rapidly to the level
326 smaller than the simulated slopes. The rapid change of the slope with AOD can be
327 related to the variation of SSA at different AOD level. Figure 6 presents the
328 relationship between SSA and AOD based on observed data in August 2012. The
329 result suggests a significant correlation between SSA and AOD. With the increase in
330 AOD, SSA is elevated; meanwhile, the slope of SSA vs AOD is gradually reduced.
331 SSA characterizes the ratio of the scattering extinction coefficient to the total
332 extinction coefficient (scattering extinction coefficient plus absorptive extinction
333 coefficient) of aerosols. The smaller the SSA, the higher the absorptive component
334 and lower the scattering component of the aerosol, and the stronger the ability of the
335 aerosol to reduce the actinic flux (Dickerson et al., 1997). Figure 6 indicates that
336 aerosols in Beijing under low AOD conditions had a higher proportion of absorptive
337 aerosol components than under high AOD conditions, and, as a result, had a stronger
338 ability to reduce the photolysis frequencies, which contributed to the rapidly reduced
339 slope of $j(\text{O}^1\text{D})$ vs AOD with AOD. However, due to absence of more SSA data of the
340 period 2012-2015, we can't give more sufficient evidence for the dependence of SSA
341 on AOD. For another perspective, Owing to the biomass burning and soot emission
342 generated from heating, the fine mode heavily-absorbing aerosol percentage is higher
343 in winter than in summer (Zheng et al., 2017; Liu et al., 2016; Zhang et al., 2013), and



344 thus aerosols in winter have stronger ability to reduce the photolysis frequencies.

345 High AOD levels often appeared in summer and low AOD levels occurred mostly in

346 winter (Figure 2), another fact that may also explains the rapidly reduced slope of

347 $j(\text{O}^1\text{D})$ vs AOD with AOD.

348 Comparing panels a and b of Figure 4, we see that at AOD smaller than 1, the

349 slope of $j(\text{O}^1\text{D})$ vs AOD exhibits a significant dependence on SZA and the slope at 30°

350 of SZA is about 1.5-2.0 times larger than that at 60° of SZA. This result is similar to

351 that of the observations made in the central Mediterranean (Casasanta et al., 2011).

352 For the purpose of comparison with the study in the Mediterranean, the slope of $j(\text{O}^1\text{D})$

353 vs AOD was calculated at AOD smaller than 0.7.

354 Table 3 presents slope, intercept and the determination coefficient (r^2) of linear

355 fits of correlation between $j(\text{O}^1\text{D})$ and AOD for each ozone column class at AOD

356 smaller than 0.7. At SZA of 60° and O_3 column concentration of 300-330 DU, the

357 respective slope of the linear regression indicates a reduction of $j(\text{O}^1\text{D})$ by $4.21 \cdot 10^{-6}$

358 s^{-1} per AOD unit. Gerasopoulos et al. (2012) reported that the observed slope in the

359 eastern Mediterranean was equal to $2.44 \cdot 10^{-6} \text{ s}^{-1}$ at O_3 column of 300-320 DU.

360 Casasanta et al. (2011) reported that the observed slope in the central Mediterranean

361 varied from $2.66 \cdot 10^{-6} \text{ s}^{-1}$ to $3.87 \cdot 10^{-6}$ at O_3 column of 300-330 DU. All of these results

362 are smaller than the value of the present study, indicating that aerosols in urban

363 Beijing had a stronger extinction capacity on $j(\text{O}^1\text{D})$ than those in the Mediterranean

364 that was influenced by both natural absorptive aerosols and anthropogenic aerosols.

365 Previous study indicated that SSA in Beijing ranged from 0.80 to 0.86 (Garland et al.,



366 2009; Han et al., 2015b; Han et al., 2017; Tian et al., 2015). The relatively low SSA in
367 Beijing could be an important reason for the stronger extinction capacity.

368

369

370 **3.3.2 The correlation between $j(\text{NO}_2)$ and AOD**

371 Unlike $j(\text{O}^1\text{D})$, $j(\text{NO}_2)$ is negligibly affected by ozone column concentration and
372 depends mainly on AOD and SZA under cloudless conditions. Figure 7 presents the
373 dependence of $j(\text{NO}_2)$ on AOD at different SZA levels under cloudless conditions.
374 The cosine of SZA ($\cos(\text{SZA})$) is categorized according to a width of 0.2. In the same
375 category of $\cos(\text{SZA})$, $j(\text{NO}_2)$ displays a strong dependence on AOD. When $\cos(\text{SZA})$
376 is at its maximum level (0.8–1), the correlation between $j(\text{NO}_2)$ and AOD is close to
377 linear. When $\cos(\text{SZA})$ decreases, the correlation tends to be nonlinear. Similar to
378 $j(\text{O}^1\text{D})$, the observed slopes of $j(\text{NO}_2)$ vs AOD are also larger than TUV-simulated
379 slope at SSA of 0.95 and 0.85 when AOD is smaller than 0.8, and decreased rapidly
380 with increasing AOD (panels c and d of Figure 5). The reason for this result is the
381 same with that for $j(\text{O}^1\text{D})$ as explained above.

382 Table 4 presents the slope, intercept and the determination coefficient (r^2) of
383 linear fits of correlation between $j(\text{NO}_2)$ and AOD for each ozone column class at
384 AOD smaller than 0.7. The slope of $j(\text{NO}_2)$ vs AOD also displays a significant
385 dependence on SZA. The slope increases as SZA increases from 0 to 0.5 and then
386 decreases as SZA increased from 0.5 to 1. At SZA of $60^\circ \pm 1$ ($\cos(\text{SZA}) = 0.5 \pm 0.015$),



387 the respective slope of the linear regression indicates a reduction of $j(\text{NO}_2)$ by $3.2 \cdot 10^{-3}$
388 s^{-1} per AOD unit. This result is larger than the value for non-dust aerosols ($2.2 \cdot 10^{-3} \text{ s}^{-1}$)
389 and close to the value for dust aerosols ($3.1 \cdot 10^{-3} \text{ s}^{-1}$) in the eastern Mediterranean
390 reported by Gerasopoulos et al. (2012).

391

392 **3.4 The parameterization relationship between photolysis frequencies, AOD, and**

393 **SZA**

394

395 As analyzed above, the photolysis frequencies ($j(\text{O}^1\text{D})$ and $j(\text{NO}_2)$) strongly
396 depended on AOD and $\cos(\text{SZA})$ and could be fit into expression E5 using a quadratic
397 polynomial form. Table 5 presents the fitting parametric equations and the
398 corresponding coefficients of determination (R^2) at different O_3 column ranges. The
399 coefficients of determination of the fitting equations are greater than 0.95 for $j(\text{NO}_2)$
400 and $j(\text{O}^1\text{D})$, indicating that both of the photolysis frequencies strongly depended on
401 AOD and $\cos(\text{SZA})$ at a certain O_3 column, and the effect of other factors such as
402 SSA and AE are integrated into the constant term in the parametric equation. Since the
403 ozone column concentration has greater influence on $j(\text{O}^1\text{D})$ than on $j(\text{NO}_2)$, the
404 parameters of fitting equations for $j(\text{NO}_2)$ are similar, but the parameters of fitting
405 equations for $j(\text{O}^1\text{D})$ have a large fluctuation at different O_3 column ranges (especially
406 a_1 and a_2). The parametric equations can be used to quantitatively evaluate the effect
407 of AOD on photolysis frequencies in Beijing. According to the parametric equations,



408 aerosols lead to a decrease in $j(\text{NO}_2)$ by 24.2% and 30.4% and a decrease in $j(\text{O}^1\text{D})$ by
409 27.3% and 32.6% in summer and winter, respectively, compared to an aerosol-free
410 atmosphere. The decreasing ratio of the photolysis frequencies in winter is higher than
411 in summer due to the higher SZA and lower SSA in winter.

412 The effect of aerosols on photolysis frequencies in Beijing is compared with
413 other studies. Real and Sartelet (2011) reported a reduction in $j(\text{NO}_2)$ and $j(\text{O}^1\text{D})$ of
414 13%-14% due to aerosols by using the radiative transfer code Fast-J during summer
415 2001 over European regions. Flynn et al (2010) reported that aerosols reduced $j(\text{NO}_2)$
416 by 3% in Huston during 2006 by using TUV model. Gerasopoulos et al (2012)
417 reported that aerosols reduced $j(\text{NO}_2)$ and $j(\text{O}^1\text{D})$ by 5%-15% with 5-yr mean AOD at
418 380nm equal to 0.27. All of these results are lower than the reduction ratio of this
419 study mainly due to higher aerosol level in Beijing (4-yr mean AOD equal to $0.76 \pm$
420 0.75). Hodzic et al. (2007) simulated a 15–30% $j(\text{NO}_2)$ photolysis reduction during
421 the 2003 European summer heatwave in the case of absorbing biomass burning
422 aerosols with AOD at 550 nm equal to 0.7-0.8 and SSA at 532 nm equal to 0.83-0.87.
423 The result of this study is comparable with the reduction ratio of this study possibly
424 due to the equivalent levels of AOD and SSA. In addition, Péré et al (2015) simulated
425 a higher reduction (20–50%) in $j(\text{NO}_2)$ and $j(\text{O}^1\text{D})$ along the transport of the aerosol
426 plume during the 2010 Russian summer wildfires episode. The higher reduction is due
427 to the higher level of AOD (peak value of AOD at 400nm reached 2-4), even though
428 SSA is very high (0.97).

429
$$j = a_1 + a_2 AOD + a_3 \cos(SZA) + a_4 (AOD)^2 + a_5 AOD \cos(SZA) + a_6 (\cos(SZA))^2 \dots E5$$



430

431 The above established parametric relationship of $PM_{2.5}$ -AOD and
432 $j(NO_2)$ -AOD-SZA gives us a chance to estimate the effect of $PM_{2.5}$ on photolysis
433 frequencies due to aerosol light extinction.

434 **3.5 The influence of AOD on ozone production**

435

436 In order to explain the effect of aerosol light extinction on ozone production, we
437 used the data from the field observation campaign undertaken in August 2012. Ozone
438 production depends on its precursors (NO_x and VOCs), meteorological factors, and
439 solar radiation. Solar radiation is the driving force for tropospheric photochemical
440 reactions, in which $j(O^1D)$ and $j(NO_2)$ are both important for ozone production. On
441 the one hand, the increase in $j(NO_2)$ promotes the photolysis of NO_2 , thereby
442 accelerating the formation of ozone. On the other hand, the increase in $j(O^1D)$
443 accelerates the photolysis of ozone. In addition, the increase in the photolysis
444 frequencies will accelerate the photolysis of OVOC (especially formaldehyde and
445 acetaldehyde), HONO, and H_2O_2 , resulting in increases in OH and HO_2 , which will
446 promote the reaction between OH and VOCs and thus produce more RO_2 . As a result,
447 more ozone is produced by increasing the reaction rate between RO_2 (or HO_2) and NO.
448 However, the increase in OH and HO_2 also consumes ozone and NO_2 , which
449 contributes to the increase in $D(O_3)$. In brief, the overall effect of changes in



450 photolysis frequencies on sources and sinks of ozone determines the change in the net
451 ozone production rate.

452 Ozone production ($\text{HO}_2 + \text{NO}$, $\text{RO}_2 + \text{NO}$), ozone loss ($\text{O}^1\text{D} + \text{H}_2\text{O}$, $\text{HO}_2 + \text{O}_3$,
453 $\text{O}_3 + \text{OH}$, $\text{NO}_2 + \text{OH}$, and $\text{O}_3 + \text{alkenes}$), and net ozone production rate during August
454 2012 were calculated by using the box model. We used the observed photolysis
455 frequencies (i.e. j_{obs}) and the calculated photolysis frequencies by parametric
456 equation under the condition of AOD equal to 0 (i.e. $j_{\text{AOD}=0}$), were used to
457 constrain the box model. The difference of simulated results in the two scenarios can
458 be attributed to the effect of aerosol light extinction. As a result, the presence of
459 aerosols causes a decrease in both ozone production rate and loss rate, as is shown in
460 Figure 8. Since the decreasing amplitude of the ozone production rate is far larger
461 than that of the ozone loss rate, the net production rate of ozone is reduced by 25%.
462 This reduction is comparable with the results of the study in Mexico City, where
463 aerosols caused a 20% reduction in the ozone concentrations (Castro et al., 2001).
464 Studies in Houston and Crete have shown that aerosols cause ozone production rates
465 to decrease by about 4% and 12%, respectively, which are lower than that found in
466 this study (Flynn et al., 2010; Gerasopoulos et al., 2012).

467 The ratio of the observed photolysis frequencies to the photolysis frequencies at
468 AOD equal to 0 is defined as JIF (Flynn et al., 2010). A JIF of less than 1 indicates
469 that the aerosols cause a decrease in the photolysis frequencies. Figure 9 shows the
470 relation between $P(\text{O}_3)_{j_{\text{obs}}}/P(\text{O}_3)_{j_{\text{AOD}=0}}$ (or $D(\text{O}_3)_{j_{\text{obs}}}/D(\text{O}_3)_{j_{\text{AOD}=0}}$) and JIF. The
471 majority of JIF values were less than 1, with an average of 0.72, indicating that



472 aerosols greatly attenuated photolysis frequencies due to high levels of AOD (average
473 of 1.07) and low levels of SSA (average of 0.84) during the observation period.
474 $P(O_3)_{j_obs}/P(O_3)_{j_AOD=0}$ and $D(O_3)_{j_obs}/D(O_3)_{j_AOD=0}$ are both linearly positively
475 correlated with JIF and the scatters are mostly above the 1:1 line. As can be seen from
476 the figure 9, a 30% reduction in photolysis frequencies ($JIF = 0.7$) due to the presence
477 of aerosols results in a decrease in ozone production rate and loss rate by about 26%
478 and 15%, respectively. The decreasing amplitude in the ozone production rate is
479 greater than the decrease in the ozone loss rate because the corresponding processes
480 of ozone production are all light-driven, but the corresponding processes of ozone loss
481 are not all light-driven because the reaction of O_3 with alkenes does not depend on
482 solar radiation. According to the simulated results, the reaction of ozone with alkenes
483 during this campaign accounts for 17% of total ozone loss.

484 The diurnal profile of the mean ozone production and loss rate is shown in
485 Figure 10. $P(O_3)$ peak midday in the 12:00-14:00 local hours at 31 ppb/h without
486 aerosol impact and 23 ppb/h with aerosol impact. The maximum $D(O_3)$ also occurs
487 between 12:00 and 14:00 at 4.2 ppb/h without aerosol impact and 3.5 ppb/h with
488 aerosol impact. There is little difference between aerosol-impact and aerosol-free
489 $P(O_3)$ (or $D(O_3)$) in the hours of 6:00-11:00, but the difference in the afternoon
490 (12:00-18:00) is large, indicating that the reduction effect of aerosol on ozone
491 production mainly occurs during the afternoon.

492 The above analysis focuses on the effect of aerosol on the ozone production due
493 to aerosol light extinction. However, it does not consider the close relationship



494 between aerosol and ozone's gaseous precursors in the actual atmosphere. To explain
495 this problem, we chose two adjacent days (small SZA effect) with obviously different
496 AOD levels: a clean day (A day: August 21, 2012; AOD = 0.21, $PM_{2.5}=21.6 \mu\text{g m}^{-3}$)
497 and a day with high aerosol pollution (B day; August 26, 2012; AOD = 3.2,
498 $PM_{2.5}=125.0 \mu\text{g m}^{-3}$) (Table 7). The difference in AOD between the two days can be
499 taken to represent the maximum daytime gap of AOD for this month. The ozone
500 column concentrations for these two days were 302 DU and 301 DU, respectively, of
501 which the effect on $j(O^1D)$ is negligible. Under these conditions, the $j(O^1D)$ value at
502 noon time decreases from $3.23 \times 10^5 \text{ s}^{-1}$ on A day to $1.29 \times 10^5 \text{ s}^{-1}$ on B day (i.e., a 60%
503 reduction) and the $j(\text{NO}_2)$ value at noon time decreases from $8.26 \times 10^{-3} \text{ s}^{-1}$ on A day
504 to $4.19 \times 10^{-3} \text{ s}^{-1}$ on B day (i.e., a 49.2% reduction). As shown in Table 7, B day has
505 higher AOD and higher concentrations of gaseous pollutants. The concentrations of
506 CO, NO_2 , HCHO and the OH reactivity of VOCs in B day are much higher than in A
507 day, with the ratio of 3.6, 2.3, and 2.0, respectively. The simultaneous increases of
508 gaseous pollutants and AOD are due to the fact that gaseous pollutants (NO_x , SO_2 ,
509 and VOCs) emitted by major pollution sources in Beijing, including traffic and
510 industry, have undergone the processes of gas-phase oxidation and nucleation to
511 generate secondary particulate matter that contributes to aerosol light extinction.
512 Previous studies have reported that secondary particulate matter has accounted for
513 more than 60% of total particulate matter during severe smog pollution in Beijing
514 summers (Han et al., 2015a; Guo et al., 2014). In addition, several studies have shown
515 that secondary components in particulate matter (especially secondary organics and



516 ammonium sulfate) have dominated the aerosol light extinction (Han et al., 2014; Han
517 et al., 2017; Wang et al., 2015). Observations made in Beijing during the summer of
518 2006 showed that ammonium sulfate and ammonium nitrate contributed 44.6% and
519 22.3%, respectively, to the total extinction coefficient during a severe period of smog
520 (Han et al., 2014); in the summer of 2014 in Beijing, ammonium sulfate, secondary
521 organic aerosols, and ammonium nitrate contributed 30%, 22%, and 18%, respectively,
522 to the total extinction coefficient (Han et al., 2017).

523 As shown in Figure 11, the simulation results indicate that the net $P(O_3)$ of B day
524 is 36.2% higher than that of A day due to higher concentrations of ozone precursors
525 on B day. This result is consistent with the observed ozone concentrations, of which
526 the observed ozone concentration in B day is 2.2 times higher than that of A day. If we
527 adjust the photolysis frequencies level of B day to the level of A day, the net $P(O_3)$
528 increases by 70.0%, which indicates that the high level of particulate matter in B day
529 greatly inhibits ozone production. This result means that the system is under negative
530 feedback, thus keeping O_3 at a relatively stable level. Table 8 summarizes the average
531 levels of gaseous pollutants and photolysis frequencies for AOD less than 1 and
532 greater than 1, as measured during August 2012. It shows that, the concentrations of
533 ozone's precursors are higher and the photolysis frequencies are lower at high AOD
534 levels ($AOD > 1$) than those at low AOD level ($AOD < 1$). This result means that the
535 negative feedback mechanism is prevalent throughout the whole campaign period.
536 Therefore, the prevention and control measures of air pollution in Beijing need to
537 incorporate this coupling mechanism between particulate matter and ozone to achieve



538 effective control of these two main pollutants.

539 **4. Conclusion**

540 Photolysis reactions are important driving forces for tropospheric photochemical
541 oxidation processes and ozone production. In this study, we explored in detail the
542 effects of aerosols on photolysis frequencies and ozone production in Beijing, based
543 on a long observation period of 4 years. We have found that:

544 (1) There is a strong correlation between $PM_{2.5}$ and AOD, and the slope in
545 summer is smaller significantly than in winter, which indicates that aerosols
546 in summer have a more efficient extinction capacity than in winter.

547 (2) As AOD increased, the extinction effect of aerosol on photolysis frequencies
548 was decreased; this result was related to a higher proportion of scattering
549 aerosols under high AOD conditions than under low AOD conditions. The
550 slope of the correlation between photolysis frequencies and AOD indicates
551 that the aerosols in urban Beijing have a stronger extinction on actinic flux
552 than absorptive dust aerosols in the Mediterranean.

553 (3) The influence of AOD on photolysis frequencies was evaluated quantitatively
554 by establishing parametric equations. According to the parametric equation,
555 aerosols lead to a decrease in $j(NO_2)$ by 24.2% and 30.4% for summer and
556 winter, respectively, and the corresponding decrease in $j(O^1D)$ by 27.3% and
557 32.6% respectively, compared to an aerosol-free atmosphere.



558 (4) In order to evaluate the effects of aerosols on ozone production rate, we
559 carried out an observation campaign in August 2014. The results show that
560 aerosols reduced the net ozone production rate by 25% by reducing the
561 photolysis frequencies. High concentrations of ozone gaseous precursors
562 were often accompanied by high concentrations of particulate matter, which,
563 to a large extent, inhibited excessive levels of ozone generation and reflected
564 the negative feedback effect of the atmospheric system. Therefore, the
565 influence of aerosol on photolysis frequencies and thus on the rate of
566 oxidation of VOCs and NO_x to ozone and secondary aerosol is important for
567 determining the atmospheric effects of controlling the precursor emissions of
568 these two important air pollutants (aerosols and ozone).

569

570 **Author contribution**

571

Author	Contribution
Wenjie Wang	acquisition of data; analysis and interpretation of data; drafting the article and revising it critically
Min Shao	substantial contributions to conception and design; revising the article critically
Min Hu	collection of data
Limin Zeng	collection of data
Yusheng Wu	collection of data

572

573



574

575

576

577 **ACKNOWLEDGEMENTS**

578 This work was supported by the Major Program of the National Natural Science

579 Foundation of China [Grant number 91644222]. We thank Hongbin Chen and Philippe

580 Goloub for data management of AOD and other aerosol optical properties on

581 AERONET.

582

583

584

585

586

587

588

589

590

591

592

593

594

595

596



597 **Reference**

- 598 Barnarda, J. C., Chapman E G., Fasta, J. D., Schmelzera, J. R., Slusserb, J. R.,
599 Shetterc, R. E.: An evaluation of the FAST-Jphotolysis algorithm for predicting
600 nitrogen dioxide photolysis rates under clear and cloudy sky conditions,
601 ATMOSPHERIC ENVIRONMENT, 38, 3393-3403,
602 10.1016/j.atmosenv.2004.03.034, 2004.
- 603 Bohn, B., Corlett, G. K., Gillmann, M., Sanghavi, S., Stange, G., Tensing, E.,
604 Vrekoussis, M., Bloss, W. J., Clapp, L. J., Kortner, M., Dorn, H. P., Monks, P. S.,
605 Platt, U., Plass-Dulmer, C., Mihalopoulos, N., Heard, D. E., Clemmshaw, K. C .,
606 Meixner, F. X., Prevot, A. S. H., Schmitt, R.: Photolysis frequency measurement
607 techniques: Results of a comparison within the ACCENT project,
608 ATMOSPHERIC CHEMISTRY AND PHYSICS, 8, 5373–5391,
609 doi:10.5194/acp-8-5373-2008, 2008.
- 610 Casasanta, G., di Sarra, A., Meloni, D., Monteleone, F., Pace, G., Piacentino, S.,
611 Sferlazzo, D.: Large aerosol effects on ozone photolysis in the Mediterranean,
612 ATMOSPHERIC ENVIRONMENT, 45, 3937-3943,
613 10.1016/j.atmosenv.2011.04.065, 2011.
- 614 Castro, T., Madronich, S., Rivale, S., Muhlia, A., Mar, B.: The influence of aerosols
615 on photochemical smog in Mexico City, ATMOSPHERIC ENVIRONMENT, 35,
616 1765-1772, 10.1016/S1352-2310(00)00449-0, 2001.
- 617 Chang, D, Song, Y, Liu, B.: Visibility trends in six megacities in China 1973–2007,
618 ATMOSPHERIC RESEARCH, 94, 161-167, 10.1016/j.atmosres.2009.05.006,
619 2009.
- 620 Che, H., Zhang, X., Li, Y., Zhou, Z., Qu, J. J., Hao, X.: Haze trends over the capital
621 cities of 31 provinces in China, 1981–2005, THEORETICAL AND APPLIED
622 CLIMATOLOGY, 97, 235-242, 10.1007/s00704-008-0059-8, 2009.
- 623 de Miranda, R., Andrade, M. F., Fattori, A. P.: Preliminary studies of the effect of
624 aerosols on nitrogen dioxide photolysis rates in the city of Sao Paulo, Brazil.



- 625 ATMOSPHERIC RESEARCH, 75, 135–148, 10.1016/j.atmosres.2004.12.004,
626 2005.
- 627 Dickerson, R. R., Kondragunta, S., Stenchikov, G., Civerolo, K. L., Doddridge, B. G.,
628 Holben, N.: The impact of aerosols on solar ultraviolet radiation and
629 photochemical smog, *Science*, 278, 827–830, 10.1126/science.278.5339.827,
630 1997.
- 631 Ehhalt, D. H., Rohrer, F.: Dependence of the OH concentration on solar UV,
632 JOURNAL OF GEOPHYSICAL RESEARCH-ATMOSPHERES, 105,
633 3565-3571, 10.1029/1999JD901070, 2000.
- 634 Finlayson-Pitts, B. J., Pitts, J. N.: Chemistry of the Upper and Lower Atmosphere.
635 Academic Press, New York, 2000.
- 636 Flynn, J., Lefer, B., Rappenglück, B., Leuchner, M., Perna, R., Dibb, J., Ziemba, L.,
637 Anderson, C., Stutz, J., Brune, W., Ren, X. R.: Impact of clouds and aerosols on
638 ozone production in Southeast Texas. *ATMOSPHERIC ENVIRONMENT*, 44,
639 4126–4133, 10.1016/j.atmosenv.2009.09.005, 2010.
- 640 Fotiadi, A., Hatzianastassiou, N., Drakakis, E., Matsoukas, C., Pavlakis, K. G.,
641 Hatzidimitriou, D., Gerasopoulos, E., Mihalopoulos, N., Vardavas, I.: Aerosol
642 physical and optical properties in the eastern Mediterranean Basin, Crete, from
643 Aerosol Robotic Network data, *ATMOSPHERIC CHEMISTRY AND PHYSICS*,
644 6, 5399–5413, 10.5194/acp-6-5399-2006, 2006
- 645 Gao W, Tie X X, Xu J M, Huang R J, Mao X Q, Zhou G Q, Luyu Chang. Long-term
646 trend of O₃ in a mega City (Shanghai), China: Characteristics, causes, and
647 interactions with precursors. *SCIENCE OF THE TOTAL ENVIRONMENT*, 603,
648 425–433, 10.1016/j.scitotenv.2017.06.099, 2017.
- 649 Garland, R.; O. Schmid, A.; Nowak, P.; Achtert, A.; Wiedensohler, S.; Gunthe, N.;
650 Takegawa, K.; Kita, Y.; Kondo, and M. Hu (2009), Aerosol optical properties
651 observed during Campaign of Air Quality Research in Beijing 2006
652 (CAREBeijing-2006): Characteristic differences between the inflow and outflow



- 653 of Beijing city air, JOURNAL OF GEOPHYSICAL
654 RESEARCH-ATMOSPHERES, 114, D00G04, 10.1029/2008JD010780, 2009.
- 655 Gerasopoulos, E., Kazadzis, S., Vrekoussis, M., Kouvarakis, G., Liakakou, E.,
656 Kouremeti, N., Giannadaki, D., Kanakidou, M., Bohn, B., Mihalopoulos, N.:
657 Factors affecting O₃ and NO₂ photolysis frequencies measured in the eastern
658 Mediterranean during the five-year period 2002–2006, JOURNAL OF
659 GEOPHYSICAL RESEARCH-ATMOSPHERES, 117, D22305,
660 10.1029/2012JD017622, 2012.
- 661 Goliff, W. S., Stockwell, W. R., Lawson, C. V.: The regional atmospheric chemistry
662 mechanism, version 2, ATMOSPHERIC ENVIRONMENT, 68: 174–185,
663 10.1016/j.atmosenv.2012.11.038, 2013.
- 664 Guo, S., Hu M, Zamora, M. L., Peng, J. F., Shang, D. J., Zheng, J., Du, Z. F., Wu, Z.
665 J., Shao, M., Zeng, L. M., Molina, M. J., Zhang, R. Y.: Elucidating severe urban
666 haze formation in China, PROCEEDINGS OF THE NATIONAL ACADEMY
667 OF SCIENCES OF THE UNITED STATES OF AMERICA, 111: 17373–17378,
668 10.1073/pnas.1419604111, 2014.
- 669 Han, T. T., Liu, X. G., Zhang, Y. H., Qu, Y., Gu, J. W., Ma, Q., Lu, K. D., Tian, H. Z.,
670 Chen, J., Zeng, L. M.: Characteristics of aerosol optical properties and their
671 chemical apportionments during CAREBeijing 2006, AEROSOL AND AIR
672 QUALITY RESEARCH, 14: 1431–1442, 10.4209/aaqr.2013.06.0203, 2014.
- 673 Han, T. T., Xu, W. Q., Chen, C., Liu, X. G., Wang, Q. Q., Li, J., Zhao, X. J., Du, W.,
674 Wang, Z. F., Sun, Y. L.: Chemical apportionment of aerosol optical properties
675 during the Asia-Pacific Economic Cooperation summit in Beijing, China,
676 JOURNAL OF GEOPHYSICAL RESEARCH-ATMOSPHERES, 120,
677 10.1002/2015JD023918, 2015b.
- 678 Han, T. T., Xu, W. Q., Li, J., Freedman, A., Zhao, J., Wang, Q. Q., Chen, C., Zhang, Y.
679 J., Wang, Z. F., Fu, P. Q.: Aerosol optical properties measurements by a CAPS
680 single scattering albedo monitor: Comparisons between summer and winter in
681 Beijing, China, JOURNAL OF GEOPHYSICAL RESEARCH-ATMOSPHERES,



- 682 122, 2513-2526, 10.1002/2016JD025762, 2017.
- 683 Han, T., Liu, X., Zhang, Y., Qu, Y., Zeng, L., Hu, M., Zhu, T.: Role of secondary
684 aerosols in haze formation in summer in the Megacity Beijing, JOURNAL OF
685 ENVIRONMENTAL SCIENCES, 31, 51-60, 10.1016/j.jes.2014.08.026, 2015a.
- 686 He, S., Carmichael, G. R.: Sensitivity of photolysis rates and ozone production in the
687 troposphere to aerosol properties, JOURNAL OF GEOPHYSICAL
688 RESEARCH-ATMOSPHERES, 104, 26307–26324, 10.1029/1999JD900789,
689 1999.
- 690 Hendrick, F; Muller, JF; Clemer, K; Wang, P; De Maziere, M; Fayt, C; Gielen, C;
691 Hermans, C; Ma, JZ; Pinardi, G; Stavrou, T; Vlemmix, T; Van Roozendael, M.,
692 Four years of ground-based MAX-DOAS observations of HONO and NO₂ in the
693 Beijing area. ATMOSPHERIC CHEMISTRY AND PHYSICS, 14(2), 765-781,
694 2014.
- 695 Hodzic, A., Madronich, S., Bohn, B., Massie, S., Menut, L., and Wiedinmyer, C.:
696 Wildfire particulate matter in Europe during summer 2003: meso-scale modeling
697 of smoke emissions, trans-*port* and radiative effects, ATMOSPHERIC
698 CHEMISTRY AND PHYSICS, 7, 4043–4064, 10.5194/acp-7-4043-2007, 2007.
- 699 Hofzumahaus, A., Kraus, A., Muller, M.: Solar actinic flux spectroradiometry: A
700 technique for measuring photolysis frequencies in the atmosphere, APPLIED
701 OPTICS, 38, 4443–4460, 10.1364/AO.38.004443, 1999.
- 702 Hofzumahaus, A., Lefer, B. L., Monks, P. S., Hall, S. R., Kylling, A., Mayer, B.,
703 Shetter, R. E., Junkermann, W., Bais, A., Calvert, J. G., Cantrell, C. A.,
704 Madronich, S., Edwards, G. D., Kraus, A.: Photolysis frequency of O₃ to O(¹D):
705 Measurements and modeling during the International Photolysis Frequency
706 Measurement and Modeling Intercomparison (IPMMI), JOURNAL OF
707 GEOPHYSICAL RESEARCH-ATMOSPHERES, 109 (D8), D08S90,
708 10.1029/2003JD004333, 2004.
- 709 Jacobson, M, Z.: Studying the effects of aerosols on vertical photolysis rate
710 coefficient and temperature profiles over an urban airshed, JOURNAL OF



- 711 GEOPHYSICAL RESEARCH-ATMOSPHERES, 103, 10593–10604,
712 10.1029/98JD00287, 1998.
- 713 Lefer, B. L., Shetter, R. E., Hall, S. R.: Impact of clouds and aerosols on photolysis
714 frequencies and photochemistry during TRACE-P: 1. Analysis using radiative
715 transfer and photochemical box models, JOURNAL OF GEOPHYSICAL
716 RESEARCH-ATMOSPHERES, 108, 8821-8835, 10.1029/2002JD003171, 2003.
- 717 Li C C, Mao J T, Liu Q H. Using MODIS to study the distribution and seasonal
718 variation of aerosol optical thickness in eastern China. Science Bulletin (China),
719 48: 2094-2100. 2003.
- 720 Li, J., Wang, Z. F., Wang, X., Yamaji, K., Takigawa, M., Kanaya, Y., Pochanart, P.,
721 Liu, Y., Irie, H., Hu, B., Tanimoto, H., Akimoto, H.: Impacts of aerosols on
722 summertime tropospheric photolysis frequencies and photochemistry over
723 Central Eastern China, ATMOSPHERIC ENVIRONMENT, 45: 1817-1829,
724 10.1016/j.atmosenv.2011.01.016, 2011.
- 725 Liao, H., Yung, Y. L., and Seinfeld, J. H.: Effects of aerosols on tropospheric
726 photolysis rates in clear and cloudy atmospheres, JOURNAL OF
727 GEOPHYSICAL RESEARCH, 104(D19), 23697–23707, 1999.
- 728 Liu, Q.Y., Ma, T. M., Olson, M. R., Liu, Y. J., Zhang, T. T., Wu, Y., Schauer, J. J.:
729 Temporal variations of black carbon during haze and non-haze days in Beijing,
730 SCIENTIFIC REPORTS, 6, 33331, 10.1038/srep33331, 2016.
- 731 Lou, S. J; Liao, H; Zhu, B. Impacts of aerosols on surface-layer ozone concentrations
732 in China through heterogeneous reactions and changes in photolysis rates.
733 ATMOSPHERIC ENVIRONMENT, 48:123-138,
734 0.1016/j.atmosenv.2013.12.004, 2014.
- 735 Lu, K. D., Rohrer, F., Holland, F., Fuchs, H., Bohn, B., Brauers, T., Chang, C. C.,
736 Häseler, R., Hu, M., Kita, K., Kondo, Y., Li, X., Lou, S. R., Nehr, S., Shao, M.,
737 Zeng, L. M., Wahner, A., Zhang, Y. H., Hofzumahaus, A.: Observation and
738 modelling of OH and HO₂ concentrations in the Pearl River Delta 2006: a



- 739 missing OH source in a VOC rich atmosphere, *ATMOSPHERIC CHEMISTRY*
740 *AND PHYSICS*, 12: 1541-1569, 10.5194/acp-12-1541-2012, 2012
- 741 Ma, X. Y., Wang, J. Y., Yu, F. Q., Jia, H. L., Hu, Y. N.: Can MODIS AOD be
742 employed to derive PM_{2.5} in Beijing-Tianjin-Hebei over China?
743 *ATMOSPHERIC RESEARCH*, 181, 250-256, 10.1016/j.atmosres.2016.06.018,
744 2016.
- 745 Ma, Z. W., Hu, X. F., Huang, L., Bi, J., Liu, Y.: Estimating Ground-Level PM_{2.5} in
746 China Using Satellite Remote Sensing. *Environ Sci Technol*, 48: 7436–7444.
- 747 Madronich, S, The Atmosphere and UV-B Radiation at Ground Level, *Environmental*
748 *UV Photobiology*, doi: 0.1007/978-1-4899-2406-3_1. 1993,
- 749 Madronich, S., and S. Flocke, The role of solar radiation in atmospheric chemistry, in
750 *Environmental Photochemistry*, edited by P. Boule, pp. 1-26, Springer-Verlag,
751 New York, 1999.
- 752 Mailler, S., Menut, L., di Sarra, A. G., Becagli, S., Di Iorio, T., Bessagnet, B., Briant,
753 R., Formenti, P., Doussin, J. F., Gomez-Amo, J. L., Mallet, M., Rea, G., Siour,
754 G., Sferlazzo, D. M., Traversi, R., Udisti, R., Turquety, S.: On the radiative
755 impact of aerosols on photolysis rates: comparison of simulations and
756 observations in the Lampedusa island during the ChArMEx/ADRIMED
757 campaign, *ATMOSPHERIC CHEMISTRY AND PHYSICS*, 16(3):1219-1244,
758 10.5194/acp-16-1219-2016, 10.5194/acp-16-1219-2016, 2016.
- 759 Peeters, J., Nguyen, T. L., Vereecken, L.: HOX radical regeneration in the oxidation
760 of isoprene. *PHYSICAL CHEMISTRY CHEMICAL PHYSICS*, 11: 5935-5939,
761 10.1039/b908511d, 2009.
- 762 Pere, J. C., Bessagnet, B., Pont, V., Mallet, M., Minvielle, F.: Influence of the aerosol
763 solar extinction on photochemistry during the 2010 Russian wildfires episode,
764 *ATMOSPHERIC CHEMISTRY AND PHYSICS*, 15, 10983-10998,
765 10.5194/acp-15-10983-2015, 2015.
- 766 Raga, G. B., Castro, T., Baumgardner, D.: The impact of megacity pollution on local



- 767 climate and implications for the regional environment: Mexico City,
768 ATMOSPHERIC ENVIRONMENT, 35, 1805-1811,
769 10.1016/S1352-2310(00)00275-2, 2001.
- 770 Real, E. and Sartelet, K.: Modeling of photolysis rates over Europe: impact on
771 chemical gaseous species and aerosols, ATMOSPHERIC CHEMISTRY AND
772 PHYSICS, 11, 1711–1727, 10.5194/acp-11-1711-2011, 2011.
- 773 Rohrer, F; Lu, K. D; Hofzumahaus, A; Bohn, B ; Brauers, T ; Chang, C. C ; Fuchs, H;
774 Haseler, R; Holland, F; Hu, M., Maximum efficiency in the
775 hydroxyl-radical-based self-cleansing of the troposphere, Nature Geoscience. 7,
776 559-563, 2014.
- 777 Shetter, R. E., Muller, M.: Photolysis frequency measurements using actinic flux
778 spectroradiometry during PEM-Tropics Mission: Instrumentation description and
779 some results, JOURNAL OF GEOPHYSICAL RESEARCH-ATMOSPHERES,
780 104, 5647-5661, 10.1029/98JD01381, 1999.
- 781 Shetter, R. E.: Photolysis frequency of NO₂: measurement and modeling during the
782 International Photolysis Frequency Measurement and Modeling Intercomparison
783 (IPMMI), JOURNAL OF GEOPHYSICAL RESEARCH-ATMOSPHERES, 108,
784 8544, 10.1029/2002JD002932, 2003.
- 785 Stone, D; Whalley, L. K; Heard, D. E. Tropospheric OH and HO₂ radicals: field
786 measurements and model comparisons, Chem. Soc. Rev,41(19): 6348-6404,
787 10.1039/c2cs35140d, 2012.
- 788 Tang, Y., Carmichael, G. R., Kurata, G., Uno, I., Weber, R. J., Song, C. H., Guttikunda,
789 S. K., Woo, J. H., Streets, D. G., Wei, C., Clarke, A. D., Huebert, B., Anderson, T.
790 L.: Impacts of dust on regional tropospheric chemistry during the ACE-Asia
791 experiment: a model study with observations, JOURNAL OF GEOPHYSICAL
792 RESEARCH-ATMOSPHERES, 109, D19S21, 10.1029/2003JD003806, 2004.
- 793 Tian, P., Wang, G. F., Zhang, R. J., Wu, Y. F., Yan, P.: Impacts of aerosol chemical
794 compositions on optical properties in urban Beijing, China, PARTICUOLOGY,
795 18, 155-164, 10.1016/j.partic.2014.03.014, 2015.



- 796 Tie, X. X., Madronich, S., Walters, S., Edwards, D. P., Ginoux, P., Mahowald, N.,
797 Zhang, R. Y., Lou, C., Brasseur, G.: Assessment of the global impact of aerosols
798 on tropospheric oxidants. JOURNAL OF GEOPHYSICAL
799 RESEARCH-ATMOSPHERES, 110, D03204, 10.1029/2004JD005359, 2005.
- 800 van Donkelaar, A., Martin, R. V., Brauer, M., Kahn, R., Levy, R., Verduzco, C., and
801 Villeneuve, P. J.: Global Estimates of Ambient Fine Particulate Matter
802 Concentrations from Satellite-Based Aerosol Optical Depth: Development and
803 Application. Environmental Health Perspectives, 118, 847-855,
804 10.1289/ehp.0901623, 2010.
- 805 Verstraeten, W. W., Neu, J. L., Williams, J. E., Bowman, K. W., Worden, J. R.,
806 Boersma, K. F.: Rapid increases in tropospheric ozone production and export
807 from China. NATURE GEOSCIENCE, 8, 690-695, 10.1038/NGEO2493, 2015.
- 808 Volkamer R, Sheehy P, Molina L T, Molina M J.: Oxidative capacity of the Mexico
809 City atmosphere – Part 1: A radical source perspective, ATMOSPHERIC
810 CHEMISTRY AND PHYSICS, 10, 6969–6991, 10.5194/acp-10-6969-2010,
811 2010.
- 812 Wang, B., Shao, M., Lu, S. H., Yuan, B., Zhao, Y., Wang, M., Zhang, S. Q., Wu, D.:
813 Variation of ambient non-methane hydrocarbons in Beijing city in summer 2008,
814 ATMOSPHERIC CHEMISTRY AND PHYSICS, 10, 5911–5923,
815 10.5194/acp-10-5911-2010, 2010.
- 816 Wang, Q., Sun, Y., Jiang, Q., Du, W., Sun, C., Fu, P., Wang, Z.: Chemical
817 composition of aerosol particles and light extinction apportionment before and
818 during the heating season in Beijing, China. JOURNAL OF GEOPHYSICAL
819 RESEARCH-ATMOSPHERES, 120: 12,708-12,722, 10.1002/2015JD023871,
820 2015.
- 821 Xin, J. Y.; Gong, C. S.; Liu, Z. R.; Cong, Z. Y.; Gao, W. K.; Song, T.; Pan, Y. P.; Sun, Y.;
822 Ji, D. S.; Wang, L. L.; Tang, G. Q.; Wang, Y. S.: The observation-based
823 relationships between PM_{2.5} and AOD over China, JOURNAL OF



- 824 GEOPHYSICAL RESEARCH-ATMOSPHERES, 121, 10701-10716,
825 10.1002/2015JD024655, 2016.
- 826 Xu, J., Ma, J. Z., Zhang, X. L., Xu, X. B., Xu, X. F., Lin, W. L., Wang, Y., Meng, W.,
827 and Ma, Z. Q.: Measurements of ozone and its precursors in Beijing during
828 summertime: impact of urban plumes on ozone pollution in downwind rural
829 areas, *ATMOSPHERIC CHEMISTRY AND PHYSICS*, 11, 12241–12252,
830 10.5194/acp-11-12241-2011, 2011.
- 831 Zhang, J. P., Zhu, T., Zhang, Q. H., Li, C. C., Shu, H. L., Ying, Y., Dai, Z. P., Wang, X.,
832 Liu, X. Y., Liang, A. M., Shen, H. X., and Yi, B. Q.: The impact of circulation
833 patterns on regional transport pathways and air quality over Beijing and its
834 surroundings, *ATMOSPHERIC CHEMISTRY AND PHYSICS*, 12, 5031–5053,
835 10.5194/acp-12-5031-2012, 2012.
- 836 Zhang, L.; Shao, J.; Lu, X.; Zhao, Y.; Hu, Y.; Henze, D. K.; Liao, H.; Gong, S.; Zhang,
837 Q.: Sources and Processes Affecting Fine Particulate Matter Pollution over North
838 China: An Adjoint Analysis of the Beijing APEC Period. *ENVIRONMENTAL
839 SCIENCE & TECHNOLOGY*, 50(16), 8731-8740, 10.1021/acs.est.6b03010,
840 2016.
- 841 Zhang, Q., Yuan, B., Shao, M., Wang, X., Lu, S., Lu, K., Wang, M., Chen, L., Chang,
842 C. C., Liu, S. C.: Variations of ground-level O₃ and its precursors in Beijing in
843 summertime between 2005 and 2011, *ATMOSPHERIC CHEMISTRY AND
844 PHYSICS*, 14, 6089-6101, 10.5194/acp-14-6089-2014, 2014.
- 845 Zhang, R., Jing, J., Tao, J., Hsu, S. C., Wang, G., Cao, J., Lee, C. S. L., Zhu, L., Chen,
846 Z., Zhao, Y., Shen, Z.: Chemical characterization and source apportionment of
847 PM_{2.5} in Beijing: seasonal perspective, *ATMOSPHERIC CHEMISTRY AND
848 PHYSICS*, 13, 7053-7074, 10.5194/acp-13-7053-2013, 2013.
- 849 Zheng, C. W., Zhao, C. F., Zhu, Y. N., Wang, Y., Shi, X. Q., Wu, X. L., Chen, T. M.,
850 Wu, F., Qiu, Y. M.: Analysis of influential factors for the relationship between
851 PM_{2.5} and AOD in Beijing, *ATMOSPHERIC CHEMISTRY AND PHYSICS*, 17,
852 13473-13489, 10.5194/acp-17-13473-2017, 2017.



853

854

855

856

857

858

859 Table 1. Instruments deployed in the field campaign undertaken in August 2012 and
860 used for data analysis.

Parameters	Measurement technique	Time resolution	Detection limit	Accuracy
$j(\text{O}^1\text{D})$ and $j(\text{NO}_2)$	Spectroradiometer	10 s	/	$\pm 10\%$
O_3	UV photometry	60 s	0.5 ppbv	$\pm 5\%$
NO	Chemiluminescence	60 s	60 pptv	$\pm 20\%$
NO_2	Chemiluminescence	60 s	300 pptv	$\pm 20\%$
CO	IR photometry	60 s	4 ppb	$\pm 5\%$
SO_2	Pulsed UV fluorescence	60 s	0.1 ppbv	$\pm 5\%$
HCHO	Hantzsch fluorimetry	60 s	25 pptv	$\pm 5\%$
VOCs	GC-FID/MS	1 h	20-300 pptv	$\pm 15\sim 20\%$

861

862

863

864

865

866

867

868

869



870

871

872

873

874

875

876

877 Table 2. O₃ column concentration, temperature relative humidity and respective
878 standard deviation for different seasons.

	O ₃ column (Du)	Temperature (°C)	Relative humidity (%)
Spring	354.9±37.3	15.6±7.8	33.2±18.1
Summer	310.2±23.8	27.5±4.2	57.2±17.7
Autumn	303.8±22.8	15.5±7.4	46.4±20.6
Winter	347.2±28.2	0.53±4.24	30.4±17.6

879

880

881

882

883

884

885

886

887

888

889

890

891



892

893

894

895

896

897

898

899 Table 3. Slope, intercept and the square of correlation coefficient (r^2) of linear fits of
900 correlation between $j(\text{O}^1\text{D})$ and AOD for each ozone column class at AOD smaller
901 than 0.7.

O ₃ column (DU)	SZA=30°			SZA=60°		
	Slope (10 ⁻⁶ s ⁻¹)	Intercept (10 ⁻⁶ s ⁻¹)	r ²	Slope (10 ⁻⁶ s ⁻¹)	Intercept (10 ⁻⁶ s ⁻¹)	r ²
300-330	-6.24±1.52	25.7±0.8	0.34	-4.21±0.43	7.67±0.33	0.41
330-360	-6.50±1.43	23.2±0.6	0.40	-5.01±0.34	7.15±0.21	0.52
360-390	-9.45±1.64	20.9±0.9	0.52	-6.93±0.62	7.59±0.34	0.66

902

903

904

905

906

907

908

909

910

911



912

913

914

915

916

917

918

919

920 Table 4. Slope, intercept and the square of correlation coefficient (r^2) of linear fits of
921 correlation between $j(\text{NO}_2)$ and AOD for each ozone column class at AOD smaller
922 than 0.7.

cos(SZA)	Slope (10^{-3} s^{-1})	Intercept (10^{-3} s^{-1})	r^2
0-0.2	-1.28±0.07	1.54±0.04	0.52
0.2-0.4	-2.44±0.10	3.40±0.04	0.41
0.4-0.6	-3.20±0.09	5.49±0.04	0.49
0.6-0.8	-2.08±0.09	7.20±0.05	0.38
0.8-1.0	-1.77±0.12	8.12±0.05	0.26

923

924

925

926

927

928

929

930

931



932
 933
 934
 935
 936
 937
 938

939 Table 5. The fitting parameters a_1 - a_6 and determination coefficients of E5 for $j(\text{NO}_2)$.

O ₃ column (DU)	a_1	a_2	a_3	a_4	a_5	a_6	r^2
			$\times 10^{-3}$				
270-300	-0.20 ± 0.09	-2.1 ± 0.1	13.1 ± 0.4	0.27 ± 0.02	0.19 ± 0.09	-3.5 ± 0.3	0.96
300-330	-0.48 ± 0.07	-1.9 ± 0.1	13.3 ± 0.3	0.19 ± 0.01	0.34 ± 0.08	-3.9 ± 0.3	0.96
330-360	-0.22 ± 0.08	-2.2 ± 0.1	11.8 ± 0.3	0.42 ± 0.03	0.23 ± 0.03	-2.6 ± 0.2	0.96
360-400	-0.21 ± 0.10	-2.0 ± 0.1	12.6 ± 0.2	0.18 ± 0.02	0.39 ± 0.03	-4.0 ± 0.3	0.95

940

941 Table 6. The fitting parameters a_1 - a_6 and determination coefficients of E5 for $j(\text{O}^1\text{D})$.

O ₃ column (Du)	a_1	a_2	a_3	a_4	a_5	a_6	r^2
			$\times 10^{-6}$				
270-300	0.88 ± 0.30	-0.10 ± 0.21	-5.1 ± 0.5	0.93 ± 0.06	-8.6 ± 0.4	43.9 ± 0.8	0.96
300-330	0.58 ± 0.07	0.13 ± 0.17	-3.8 ± 0.8	0.68 ± 0.04	-7.1 ± 0.2	37.1 ± 0.8	0.96
330-360	2.2 ± 0.20	-0.65 ± 0.19	-9.8 ± 0.9	1.01 ± 0.07	-6.3 ± 0.3	38.1 ± 0.6	0.97
360-400	2.0 ± 0.10	-0.72 ± 0.40	-7.0 ± 0.5	0.76 ± 0.08	-6.2 ± 0.7	33.0 ± 0.8	0.95

942

943



944

945

946

947

948

949 Table 7. Mean and standard deviation of observed data during daytime (6:00–18:00)

950 for A day and B day.

Observed data	A day: August 21, 2012	B day: August 26, 2012
AOD	0.21 ± 0.05	3.2 ± 0.4
PM _{2.5} ($\mu\text{g m}^{-3}$)	21.6 ± 9.0	125.0 ± 15.7
O ₃ column (Du)	302 ± 3.0	301 ± 3.0
Temperature(°C)	27.6 ± 3.3	27.6 ± 3.2
Relative humidity (%)	47.6 ± 10.1	54.5 ± 11.8
$j(\text{O}^1\text{D})(\text{s}^{-1})$	$1.57 \times 10^{-5} \pm 1.24 \times 10^{-5}$	$6.87 \times 10^{-6} \pm 5.2 \times 10^{-6}$
$j(\text{NO}_2)(\text{s}^{-1})$	$5.37 \times 10^{-3} \pm 2.88 \times 10^{-3}$	$2.87 \times 10^{-3} \pm 1.65 \times 10^{-3}$
O ₃ (ppb)	39.7 ± 16.56	86.8 ± 52.82
NO ₂ (ppb)	10.7 ± 5.0	24.9 ± 9.6
CO (ppm)	0.24 ± 0.05	0.85 ± 0.14
VOC reactivity (s^{-1})	3.0 ± 0.7	6.4 ± 1.7
HCHO (ppb)	2.7 ± 1.1	7.4 ± 1.9

951

952

953



954

955

956

957 Table 8. Monthly mean and standard deviation of observed data during daytime

958 (6:00–18:00) under the condition of AOD less than 1 and larger than 1 in August 2012

Observed data	AOD<1	AOD>1
AOD	0.43 ± 0.24	2.0 ± 0.8
PM _{2.5} ($\mu\text{g m}^{-3}$)	26.4 ± 12.4	76.9 ± 47.1
O ₃ column (Du)	303 ± 4.0	302 ± 5.0
Temperature(°C)	29.6 ± 4.3	29.2 ± 4.1
Relative humidity (%)	42.1 ± 15.8	57.0 ± 12.8
j(O ¹ D)(s ⁻¹)	$1.62 \times 10^{-5} \pm 1.05 \times 10^{-5}$	$1.03 \times 10^{-5} \pm 0.67 \times 10^{-5}$
j(NO ₂)(s ⁻¹)	$5.64 \times 10^{-3} \pm 2.42 \times 10^{-3}$	$3.80 \times 10^{-3} \pm 1.66 \times 10^{-3}$
O ₃ (ppb)	52.4 ± 33.8	67.9 ± 45.7
NO ₂ (ppb)	16.4 ± 7.8	24.4 ± 8.9
CO (ppm)	0.47 ± 0.20	0.95 ± 0.47
VOC reactivity (s ⁻¹)	4.3 ± 1.7	6.2 ± 2.2
HCHO (ppb)	4.0 ± 1.4	6.5 ± 1.9

959

960

961

962

963

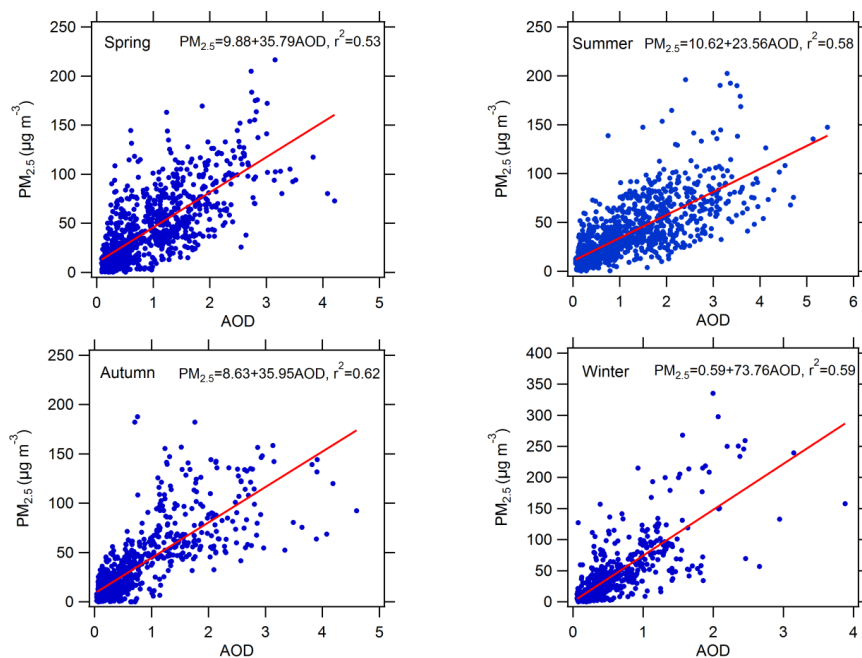
964



965

966

967



968

969 Figure 1. Scatter plots between AOD at 380nm and PM_{2.5} in four different seasons.

970 The slope, intercept and determination coefficient (r^2) were calculated.

971

972

973

974

975

976

977

978

979

980

981

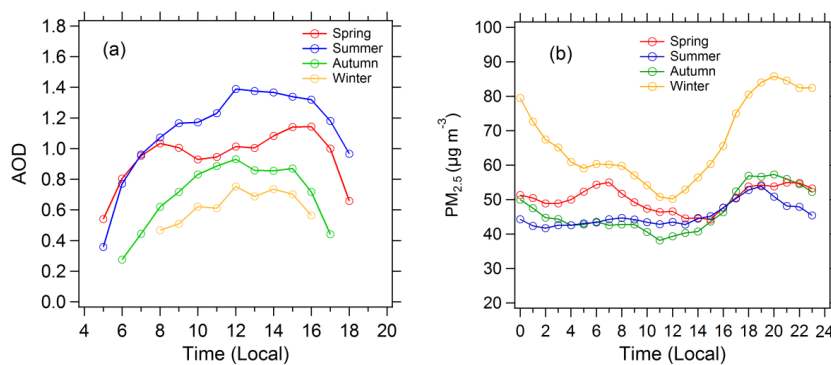


982

983

984

985



986

987 Figure 2. Diurnal cycles of (a) AOD and (b) PM_{2.5} in the four seasons.

988

989

990

991

992

993

994

995

996

997

998

999

1000

1001

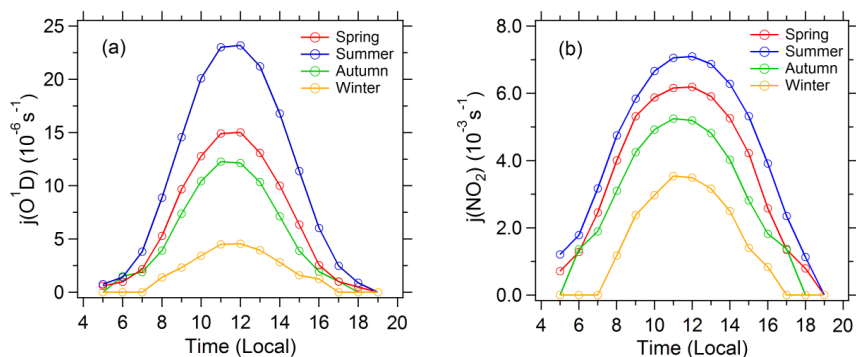
1002

1003

1004



1005
1006
1007
1008



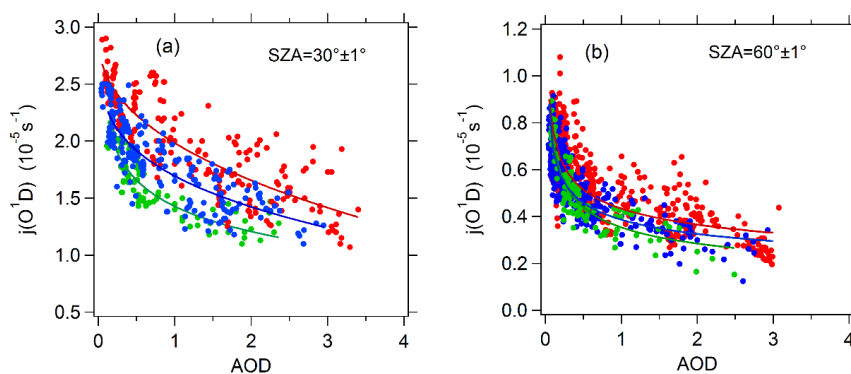
1009

1010 Figure 3. Diurnal cycles of (a) $j(\text{O}^1\text{D})$ and (b) $j(\text{NO}_2)$ in the four seasons under
1011 cloudless conditions.

1012
1013
1014
1015
1016
1017
1018
1019
1020
1021
1022
1023
1024
1025
1026



1027
1028
1029
1030
1031
1032



1033

1034 Figure 4. Dependence of $j(\text{O}^1\text{D})$ on AOD at SZA of (a) 30° and (b) 60° and at
1035 different classes of ozone column concentration: 300-330 DU (red), 330-360 DU
1036 (blue), and 360-390 DU (green).

1037
1038
1039
1040
1041
1042
1043
1044
1045
1046
1047



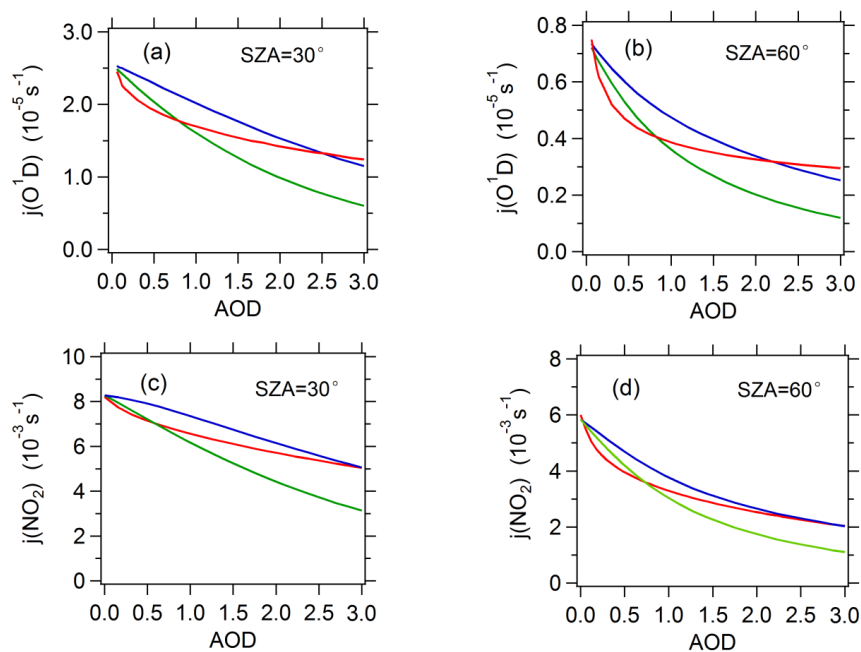
1048

1049

1050

1051

1052



1053

1054 Figure 5. The relationship between observed or TUV-simulated photolysis

1055 frequencies and AOD at SZA of 30° and 60°. The red line represents observed

1056 average photolysis frequencies; the blue line and green line represents TUV-simulated

1057 photolysis frequencies at SSA of 0.95 and 0.85 respectively.

1058

1059

1060

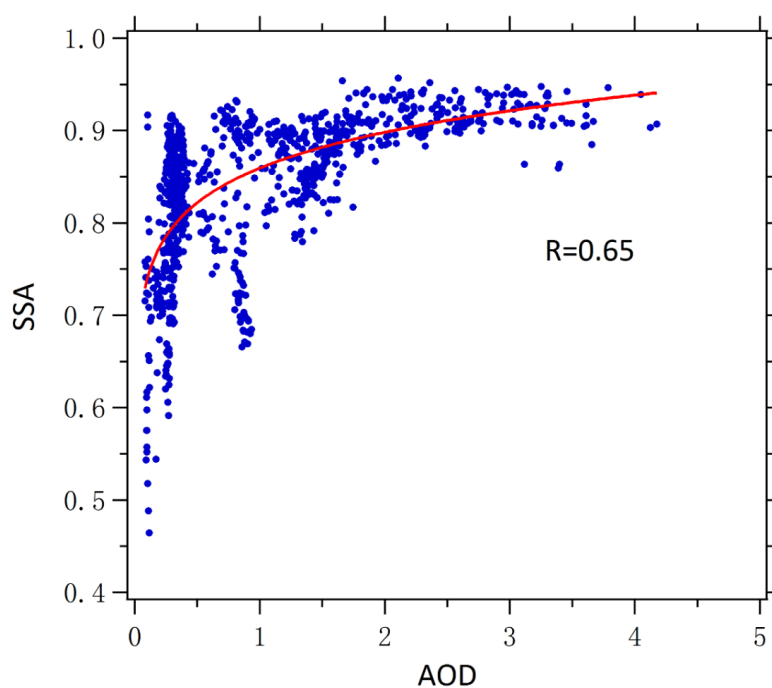
1061

1062

1063



1064
1065
1066
1067
1068

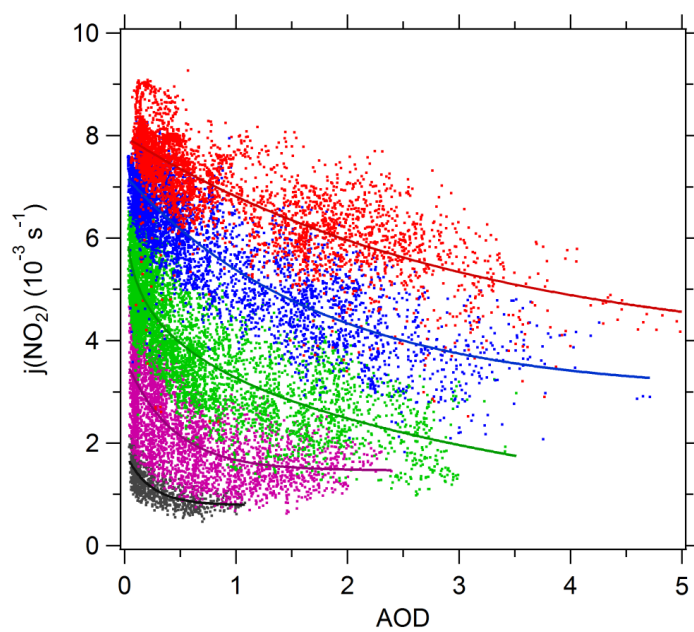


1069
1070
1071
1072
1073
1074
1075
1076
1077
1078
1079

Figure 6. Correlation between SSA and AOD observed in August 2012.



1080
1081
1082
1083
1084

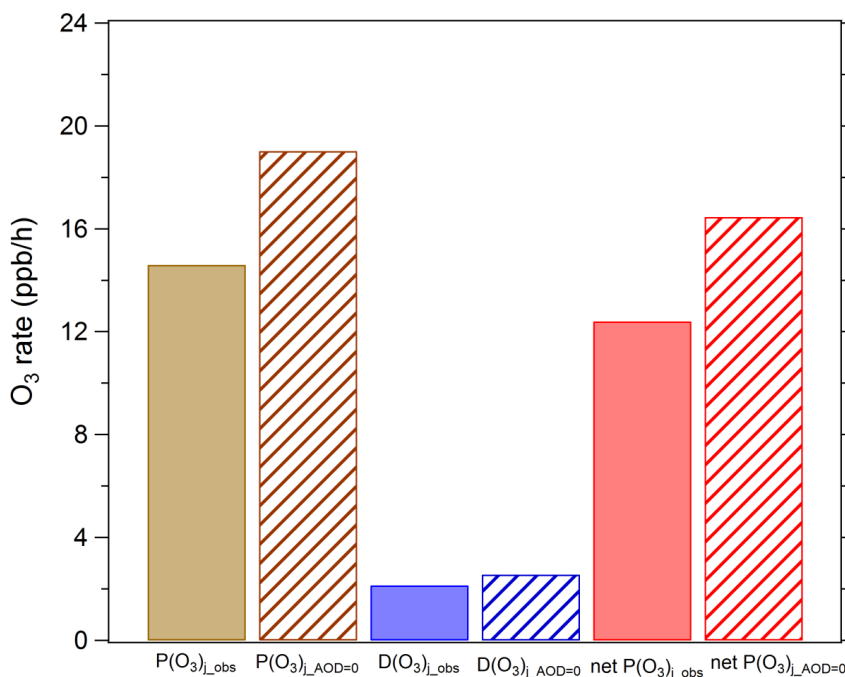


1085
1086
1087
1088
1089
1090
1091
1092
1093
1094
1095
1096

Figure 7. Dependence of $j(\text{NO}_2)$ on AOD at different SZA classes. The classes of $\cos(\text{SZA})$ are 0–0.2 (black), 0.2–0.4 (purple), 0.4–0.6 (green), 0.6–0.8 (blue), and 0.8–1 (red).



1097
1098
1099



1100

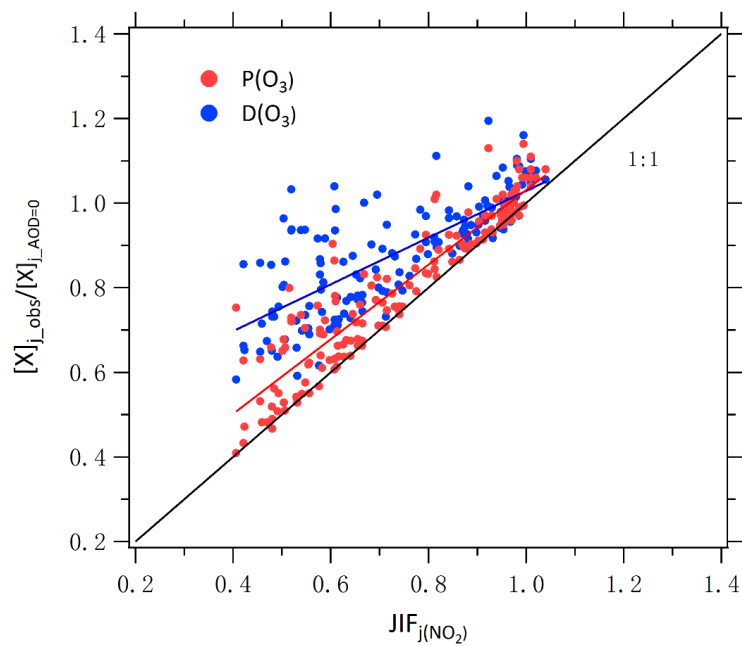
1101 Figure 8. Average ozone production and loss terms in August 2012. $P(O_3)_{j_obs}$,
1102 $D(O_3)_{j_obs}$ and net $P(O_3)_{j_obs}$ represents ozone production rate, ozone loss rate, and net
1103 ozone production rate under observed photolysis frequencies; $P(O_3)_{j_AOD=0}$, $D(O_3)$
1104 $_{j_AOD=0}$ and net $P(O_3)_{j_AOD=0}$ represents ozone production rate, ozone loss rate, and net
1105 ozone production rate under calculated photolysis frequencies when AOD is equal to
1106 0.

1107
1108
1109
1110



1111

1112



1113

1114 Figure 9. Correlation between $P(O_3)_{j_obs}/P(O_3)_{j_AOD=0}$ (or $D(O_3)_{j_obs}/D(O_3)_{j_AOD=0}$) and

1115 JIF of $j(NO_2)$.

1116

1117

1118

1119

1120

1121

1122

1123

1124

1125

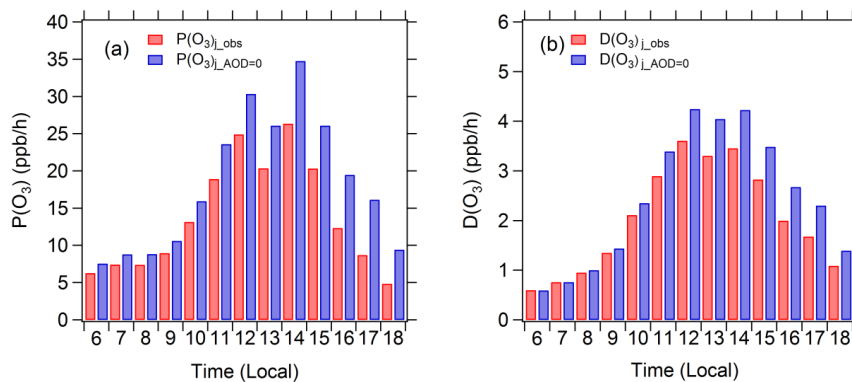
1126

1127



1128

1129



1130

1131 Figure 10. Diurnal profiles of mean $P(O_3)_{j_obs}$, $P(O_3)_{j_AOD=0}$, $D(O_3)_{j_obs}$, and

1132 $D(O_3)_{j_AOD=0}$.

1133

1134

1135

1136

1137

1138

1139

1140

1141

1142

1143

1144

1145

1146

1147

1148

1149

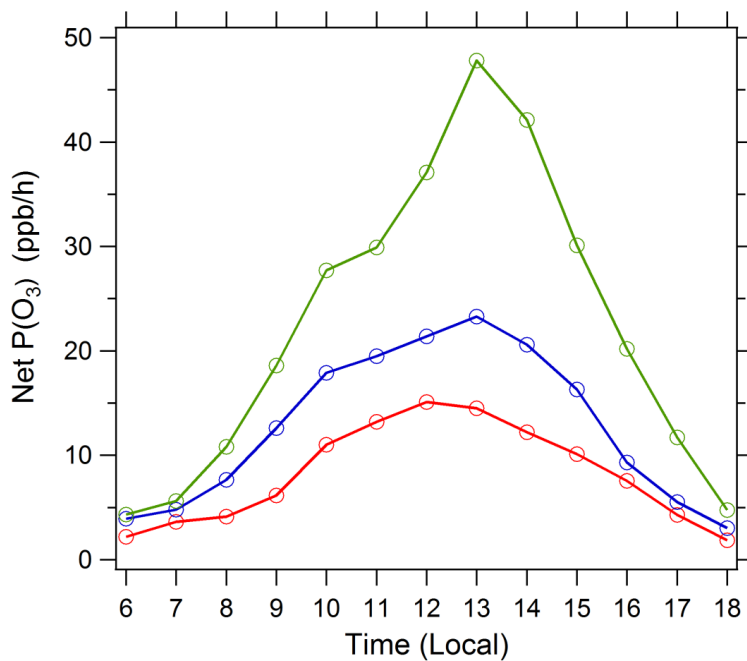


1150

1151

1152

1153



1154

1155 Figure 11. Diurnal profile of net P(O₃) simulated by the box model. Three cases are

1156 displayed: (1) A day (red circles); (2) B day (blue circles); and (3) the photolysis

1157 frequencies of B day adjusted to the level of A day with other conditions unchanged

1158 (green circles).

1159